In Vivo Pharmacokinetics, Long-Term Biodistribution, and Toxicology of PEGylated Graphene in Mice

Kai Yang,[†,⊥] Jianmei Wan,[‡,⊥] Shuai Zhang,[†] Youjiu Zhang,[‡,*] Shuit-Tong Lee,[§] and Zhuang Liu[†,*]

[†]Jiangsu Key Laboratory for Carbon-Based Functional Materials & Devices, Institute of Functional Nano & Soft Materials (FUNSOM), Soochow University, Suzhou, Jiangsu 215123, China, [‡]School of Radiation Medicine and Public Health Soochow University, Suzhou, Jiangsu 215123, China, and [§]Center of Super-Diamond and Advanced Films (COSDAF) and Department of Physics and Materials Science, City University of Hong Kong, Hong Kong SAR, China. [⊥]These two authors contributed equally to this work.

ABSTRACT Graphene has emerged as interesting nanomaterials with promising applications in a range of fields including biomedicine. In this work, for the first time we study the long-term *in vivo* biodistribution of ^{125}I-labeled nanographene sheets (NGS) functionalized with polyethylene glycol (PEG) and systematically examine the potential toxicity of graphene over time. Our results show that PEGylated NGS mainly accumulate in the reticuloendothelial system (RES) including liver and spleen after intravenous administration and can be gradually cleared, likely by both renal and fecal excretion. PEGylated NGS do not cause appreciable toxicity at our tested dose (20 mg/kg) to the treated mice in a period of 3 months as evidenced by blood biochemistry, hematological analysis, and histological examinations. Our work greatly encourages further studies of graphene for biomedical applications.

I n the past decade, nanobiotechnology has been rapidly growing and has shown great potential in disease diagnosis and treatment, such as in using functional nanomaterials for cancer molecular imaging and drug delivery.[1−3] However, the pharmacokinetics, long-term fate, and potential toxicity of functional nanomaterials should be well examined before any novel nanomaterials can be translated into the clinic.[4−6] Graphene, single or few layers of sp²-bonded carbon, has attracted tremendous attention in the past few years from a number of different fields.[7−9] Although the bigger sister of graphene, carbon nanotubes rolled up by graphene layers, has been widely investigated for applications in biosensing, drug delivery, and molecular imaging,[10−18] the biomedical research on graphene has been relatively less explored until recently. Starting from 2009, a number of groups have used graphene as novel biosensing platforms for detection of biological molecules *via* different mechanisms.[19−26] In our earlier work, polyethylene glycol (PEG) functionalized

nanographene sheets (NGS) exhibiting high solubility and stability in physiological solutions were used for *in vitro* drug delivery and biological imaging.[27,28] Zhang *et al.*[29] and Yang *et al.*[30] have also developed graphene as drug carries for controlled loading and releasing of antitumor drugs. Compared with carbon nanotubes with the one-dimensional (1D) structure, the two-dimensional (2D) nanographene has unique shape/size as well as various intriguing physical and chemical properties, making it an interesting material in nanomedicine.

In our recent study, we labeled NGS-PEG with Cy7, a commonly used NIR fluorescent dye, and studied the *in vivo* behaviors of graphene by *in vivo* fluorescence imaging.[31] We uncovered the highly efficient tumor passive targeting ability of PEGylated NGS (NGS-PEG) and used graphene as a powerful photothermal therapy agent for effective photo-ablation of tumors in a mouse model.[31] Although semiquantitative biodistribution study was carried out by ex vivo fluorescence imaging in that work, the fluorescent method has many intrinsic limitations such as difficulties in quantification, light absorption and scattering by biological tissues, as well as possible photobleaching and quenching of fluorescent dyes. The quantitative *in vivo* biodistribution especially long-term biodistribution study of graphene using a more accurate and reliable method is urgently demanded in this field. The *in vivo* toxicology of graphene should also be investigated with great care. Herein, we study the pharmacokinetics and biodistribution of graphene using ^{125}I radionuclide labeled NGS-PEG and carry out a systemic toxicology examination of functionalized graphene in mice.

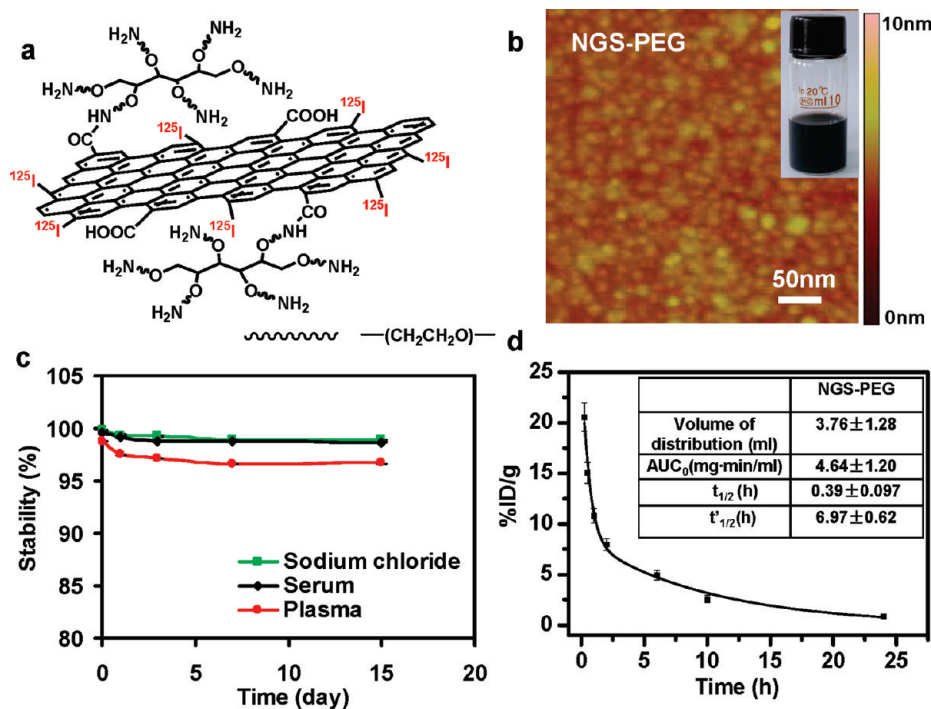*Address correspondence to
zliu@suda.edu.cn,
yjzhang@suda.edu.cn.

Figure 1. NGS functionalized with PEG and the pharmacokinetics of NGS-PEG. (a) A scheme of a graphene sheet with PEG functionalization and ^{125}I labeling. **(b)** An AFM image of NGS-PEG; (inset) a photo of a NGS-PEG solution at a concentration of 0.5 mg/mL. **(c)** The radiolabeling stability curve of ^{125}I-NGS-PEG in saline, serum, and mouse plasma at 37 °C. Error bars were based on standard deviations of triplicated measurements. **(d)** The blood circulation curve of ^{125}I-NGS-PEG. The pharmacokinetics of NGS-PEG followed a two-compartment model. Error bars were based on standard deviations of 4−5 mice per group. Inset table: pharmacokinetic data of ^{125}I-NGS-PEG including volume of distribution, AUC and circulation half-lives.

REULTS AND DISCUSSION

NGS-PEG was prepared from graphene oxide (GO) following our previous protocol.[27,28] In brief, GO was synthesized by a modified Hammer's method. Amine terminated six-arm branched PEG (10 kDa) was conjugated to GO sheets *via* amide formation to improve their biocompatibility (Figure 1a). Successful PEGylation was evidenced by the high stability of NGS-PEG in aqueous solutions with high salt contents (Supporting Information Figure S1) as well as infrared (IR) spectra (Supporting Information Figure S2). Atomic force microscope (AFM) images showed that NGS-PEG were very small sheets with a size range of *ca.* 10−30 nm (Figure 1b) and mostly single or double layered (Supporting Information Figure S3).[27,28]

In order to track graphene *in vivo*, we labeled NGS-PEG with ^{125}I using a strategy similar to the ^{125}I-labeling of carbon nanotubes (see Experimental Methods for details).[32] The X-ray photoelectron spectroscopy (XPS) confirmed the existence of iodine in our labeled NGS-PEG sample (Supporting Information Figure S4). We suggest that reactive iodine species introduced by chloramines-T oxidization of I^- are likely conjugated to the edges or detects of graphene sheets where dangling bonds exist (Figure 1a). The radiolabeling stability of ^{125}I-NGS-PEG was tested in 0.9% sodium chloride, serum as well as mouse plasma at 37 °C for 15 days (Figure 1c), revealing minimal amounts of ^{125}I detachment

from NGS-PEG (less than 5% of ^{125}I fell off from graphene in the mouse plasma at 37 °C over 15 days). The excellent radiolabeling stability of ^{125}I on NGS-PEG allows long-term tracking and detection of graphene in animals.

To understand the pharmacokinetics of ^{125}I-NGS-PEG, we first measured radioactivity levels in the blood over time (Figure 1d) after intravenous injection of ^{125}I-NGS-PEG into Balb/c mice (4 mg/kg, 20 μCi ^{125}I-NGS-PEG). Blood was drawn from the tail veins of mice at different time points postinjection (p.i.), and measured by a gamma counter. The blood circulation curve showed that the pharmacokinetics of NGS-PEG followed a two-compartment model, with the first and second phase blood circulation half-lives of 0.39 ± 0.097 and 6.97 ± 0.62 h, respectively. The volume of distribution was measured to be 3.76 ± 1.28 L and the area under curve ($AUC_{0-\infty}$) was 4.64 ± 1.20 mg · min/mL (Figure 1d).

Next, we studied the biodistribution of ^{125}I-NGS-PEG. Female Balb/c mice were sacrificed at 1 h, 6 h, 1 day, 3 days, 7 days, 15 days, 30 days, and 60 days post injection of ^{125}I-NGS-PEG (4 mg/kg, 20 μCi ^{125}I-NGS-PEG). Various organs and tissues were collected and measured by the gamma counter. It was found that NGS-PEG distributed in many different organs at 1 h p.i., but mainly accumulated in the reticuloendothelial system (RES) such as liver and spleen (Figure 2a) at later
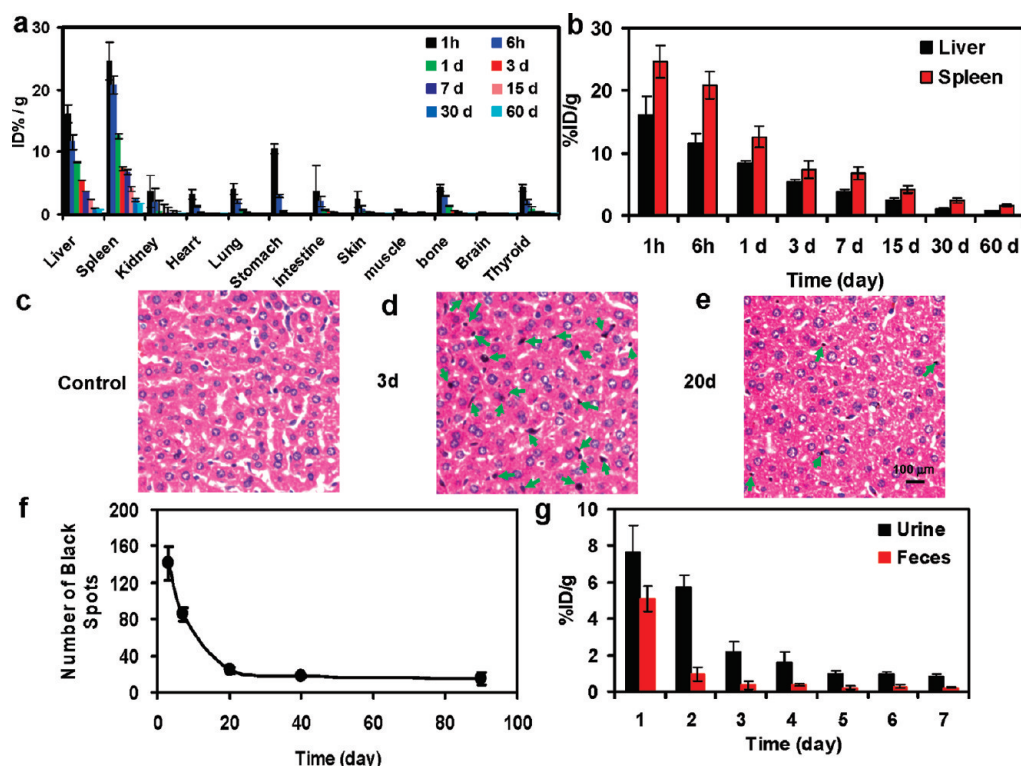
Figure 2. Biodistribution and clearance of NGS-PEG. (a) Time-dependent biodistribution of ^{125}I-NGS-PEG in female Balb/c mice. (b) ^{125}I-NGS-PEG levels in the liver and spleen over time. (c-e) H&E stained liver slices from the untreated control mice (c) and NGS-PEG injected mice at 3 d (d) and 20 d (e) p.i. Brown-black spots which could be clearly differentiated from the blue-stained cell nuclei were noted in the liver of mice 3 days after injection of graphene. Much less black spots in the liver were observed 20 days later. (f) Statistic of black spot numbers in liver slices at various time postinjection of NGS-PEG. Numbers of spots in full image fields under a 20× objective were averaged over 5 images at each data point. (g) ^{125}I-NGS-PEG levels in urine and feces in the first week after injection. Mouse excretions were collected by metabolism cages. Error bars in the above data were based on standard deviations of 4−5 mice per group.

time points. Substantial bone uptake of NGS was also noted at early time points p.i., likely owing to the macrophage uptake of nanomaterials in the bone marrow. The kidney and intestine uptake of NGS could be associated with possible renal and fecal excretion, respectively. Thyroid activity, which is normally associated with the deiodination, was also checked in our biodistribution experiments (Figure 2a). Only at the earliest time points did we notice appreciable thyroid uptake (~4%ID/g at 1 h p.i.), which corresponded to <0.05% of total injected [125]I (the mouse thyroid has an average weight of ~0.01 g). This was likely due to the small amount of unpurified free ^{125}I in the injected ^{125}I-NGS-PEG sample. Very low thyroid uptake was observed at later time points and barely detectable on and after day 3, when the liver/spleen uptakes are still substantially high, another evidence to prove the stability of ^{125}I labeling on graphene. As a control experiment, we injected free Na[125]I into female Balb/c mice via tail veins (20 μCi Na[125]I per mouse) and measured the biodistribution at 6 h p.i. (Supporting Information Figure S5). In marked contrast to the biodistribution data of ^{125}I-NGS-PEG, only low ^{125}I activity was observed in most organs including liver and spleen due to the fast renal excretion of small ^{125}I ions.

It is worth noting that low RES uptake of NGS-PEG was observed when fluorescence imaging was used to track Cy7 labeled NGS-PEG in our earlier work.[31] The quenching of Cy7 dyes in the liver and spleen is likely the reason that leads to less accurate biodistribution results by fluorescence imaging. Significantly, our current method using radiolabeled NGS obviously provides a more reliable way to study the in vivo behaviors of graphene.

From the biodistribution data, the NGS levels in most organs became very low 3 days after injection except that in the liver and spleen, in which a relatively slow but persistent decrease of ^{125}I-NGS-PEG radioactivity was also noticed (Figure 2b), suggesting possible clearance of NGS from the mouse body. However a possibility that cannot be easily excluded is the detaching of ^{125}I from the labeled NGS in the complicated in vivo environment, even though the ^{125}I labeling appears to be rather stable in vitro in the mouse plasma. Detection of graphene directly would be a more reliable way to study the clearance behaviors of this nanomaterial in addition to the radiolabeling method. A Raman spectroscopy method was previously used to quantitatively track the in vivo biodistribution of single-walled carbon nanotubes (SWNTs) in the long term.[33] Unfortunately
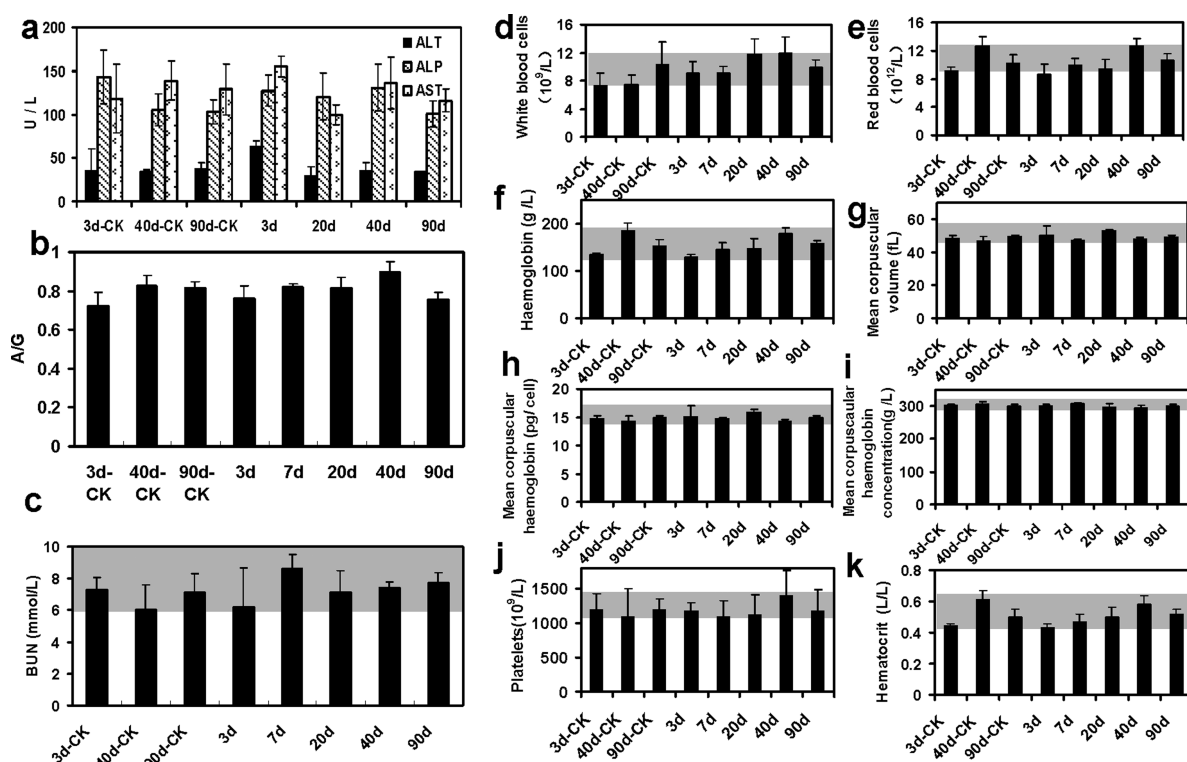
Figure 3. Blood biochemistry and hematology data of female Balb/c mice treated with NGS-PEG at the dose of 20 mg/kg at 3, 7, 20, 40, and 90 d p.i. Age-matched control untreated mice were sacrificed at 3, 40, and 90 d (3d-CK, 40d-CK, and 90d-CK). (a) ALT, ALP, and AST levels in the blood at various time points after NGS-PEG treatment. (b) Time-course Albumin/globin ratios. Blood chemistry data suggested no hepatic disorder induced by NGS-PEG treatment. (c) Blood urea nitrogen (BUN) over time. (d−k) Time-course changes of white blood cells (d), red blood cells (e), platelets (f), hemoglobin, (g), mean corpuscular volume (h), mean corpuscular hemoglobin (i), mean corpuscular hemoglobin concentration (j), and hematocrit (k) from control mice and NGS-PEG treated mice. All blood chemistry and hematological data were all within the normal range. Statistic was based on 5 mice per data point. Gray areas in the figures show the normal reference ranges of hematology data of female Balb/c mice.[35]

this method does not apply to NGS-PEG as the Raman scattering signals from oxidized graphene are orders of magnitudes lower than that of SWNTs.

To confirm the clearance of graphene, we collected the mouse liver and spleen at various time points after injection of NGS-PEG (20 mg/kg) and sliced them for Haematoxylin and Eosin (H&E) staining. Large numbers of dark borrow-black spots, which were due to accumulations of NGS and not found in the normal liver, were observed in liver slices at early time points after injection of NGS-PEG, but gradually disappeared over time (Figure 2c−e). Similar black spots or pigments were observed before in the liver of mice injected with carbon nanotubes.[6,34] We counted the total numbers of black spots over large image fields and plotted the averaged spot numbers per field against the time (Figure 2f). An obvious trend of decrease in the number of NGS aggregates in the liver was observed, consistent with the ^{125}I based biodistribution data. Only small numbers of black spots could be seen at later time points after 20 days, suggesting the clearance of NGS-PEG from the mouse liver. Brown-black pigments were also noted in the spleen splices at 3 days and 7 days p.i., however they were difficult to be differentiated from the stained spleen cell nuclei and thus could hardly be accurately

counted. We further used metabolism cages to collect urine and feces of mice after injection of ^{125}I-NGS-PEG (Figure 2g). High radioactivities were measured in urine and feces samples, suggesting that the clearance of NGS was possibly through both renal and fecal excretions.

Our NGS-PEG sample has a relatively large size distribution (10−30 nm measured by AFM). NGS-PEG with small sizes (2D sheets with diameter ~10 nm or even less) may be cleared out by renal excretion. While certain amounts of NGS-PEG (especially those with larger sizes) accumulated in the RES macrophages could be excreted *via* the biliary pathway into feces.[33] Another possibility is the gradual degradation of nanographene *in vivo* (*e.g.*, by oxidative metabolic pathways), which might also happen especially over long periods of time.

Potential long-term *in vivo* toxicity of nanomaterials, especially those that are not considered to be biodegradable, has been the major concern in the community of nanomedicine. Although no noticeable toxicity of NGS-PEG was observed in our previous work for mice in 40 days after NGS-PEG based photothermal therapy,[31] a more comprehensive time-course study is still required to uncover any potential *in vivo* toxic effect of NGS-PEG. Here, we systematically investigated the
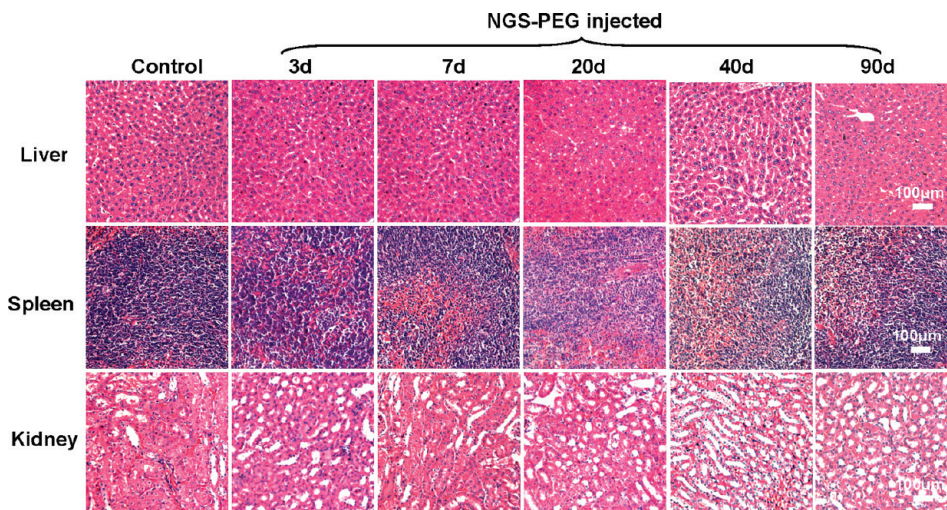
Figure 4. Representative H&E stained images of major organs including liver, spleen, and kidney collected from the control untreated mice and NGS-PEG injected mice at various time points postinjection. The dose of NGS-PEG was 20 mg/kg. No obvious organ damage or lesion was observed for NGS-PEG treated mice.

in vivo toxicology of NGS-PEG to female Balb/c mice over 3 months. During our experiments, we did not notice any obvious sign of toxic side effect for NGS-PEG injected mice at the dose of 20 mg/kg within 90 days. Neither death nor significant body weight drop was noted in the treatment group (Supporting Information Figure S6)

To reveal any potential toxic effect of NGS-PEG on the treated mice, we carried out blood biochemistry and hematology analysis. Mice injected with NGS-PEG (20 mg/kg, unlabeled) were sacrificed at 3, 7, 20, 40, and 90 days p.i. for blood collection (5 mice per group). Blood from age matched control untreated mice was collected at 3, 40, and 90 days p.i. (5 mice per group). Various biochemistry parameters were tested with particular attention paid to the liver function markers including alanine aminotransferase (ALT), aspartate aminotransferase (AST), alkaline phosphatase (ALP), and the ratio of albumin and globulin (A/G) (Figure 3 a,b).[5] No obvious hepatic toxicity was induced by NGS-PEG treatment. As an indicator of kidney functions, the urea levels in the blood of treated mice were also normal[35] (Figure 3c). For the hematological assessment, we selected the following important hematology markers: white blood cells, red blood cells, hemoglobin, mean corpuscular volume, mean corpuscular hemoglobin, mean corpuscular hemoglobin concentration, platelet count, and mean corpuscular hemoglobin (Figure 3d−k). All of the above parameters in the NGS-PEG treated groups at different time p.i. appeared to be normal compared with the control groups and in good agreement with the reference normal ranges.[35] The only slight variation was noted for white blood cell counts, which were sensitive to the bacteria infections and housing conditions, and still fell into the normal range for the treatment group.[35] No appreciable toxicity of NGS-PEG was

noted from the blood biochemistry and hematological data.

Careful necropsy was conducted 3, 7, 20, 40, and 90 days after injection of NGS-PEG (no ^{125}I labeling) at the dose of 20 mg/kg. No obvious organ damage was noticed except that the color of liver and spleen turned brown due to the accumulation of NGS in these organs, which changed back to normal colors at later time points after 20 days, another indication of NGS-PEG clearance from these organs. We collected the main organs of mice from the control and treated groups and sliced them for H&E staining. No noticeable toxic effect on organs was observed (Figure 4, Supporting Information Figure S6) at various times postinjection of NGS-PEG, except for the brown-black spots in the liver and spleen noted at early time points. Overall there were no apparent histopathological abnormalities or lesions in the treated groups at our tested NGS-PEG dose.

CONCLUSION

We for the first time studied *in vivo* long-term biodistribution of NGS-PEG by a radiolabeling method and investigated the potential time-course toxicity of NGS-PEG in female Balb/c mice. Although a fluorescent labeling and imaging method was used in our previous work to study NGS-PEG *in vivo*, the potential quenching and other intrinsic limitations of fluorescence imaging could lead to nonquantitative and less accurate biodistribution results.[31] In comparison, the pharmacokinetics and biodistribution studies based on ^{125}I-labeled NGS-PEG provide more reliable and quantitative information for the *in vivo* behaviors of biocompatibly functionalized graphene. Both biodistribution measurements based on ^{125}I labeling and observations from H&E slices suggest the gradual clearance of graphene from mice, possibly *via* both renal and fecal clearance. No obvious toxicity of NGS-PEG at

the dose of 20 mg/kg to Balb/c female mice was observed in our careful blood biochemistry, hematology, and histology analysis. However, the exact clearance mechanisms of NGS-PEG, especially the size effect of graphene sheets on their *in vivo* behaviors, would be very important and require further investigations. More careful toxicology studies of this material at higher doses and using different animal models are necessary before any potential clinical applications of graphene. Nevertheless, our results are highly encouraging and pave the way for future graphene based *in vivo* biomedical research.

EXPERIMENTAL METHODS

Synthesis of PEGylated NGS. PEGylated NGS were prepared according to our previous protocol.[27,28] An aqueous suspension (5 mL) of graphene oxide (GO) prepared by the modified Hammer's method at a concentration of ∼3 mg/mL was sonicated for about 30 min to give a clear solution. NaOH (0.12 g/mL) was added to the GO suspension and bath sonicated for about 3 h. The resulting solution was neutralized and purified by repeated rinsing and centrifugation. A solution of 6-arm-polyethylene glycol-amine (Sunbio Inc.) (3 mg/mL) was added to the GO solution (0.5 mg/mL), and the mixture was sonicated for 5 min. *N*-(3-dimethylaminopropyl-*N*′-ethylcarbodiimide) hydrochloride (EDC, from Fluka Inc.) was then added to the mixture in two equal portions to give a final concentration of 1 mg/mL totally. The reaction was allowed overnight, yielding a NGS-PEG solution which was stored at 4 °C.

[125]I Labeling of NGS-PEG. Na[125]I was obtained from Chengdu nuclear isotope Qualcomm Inc. Excess PEG in the as-synthesized NGS-PEG sample was removed by centrifuge filtration through Amicon centrifugal filters (Millipore) with 100 kDa molecular weight cut off (MWCO) and washed with water for six times. The purified NGS-PEG (2 mg/mL) was labeled by ^{125}I using a standard chloramine T oxidation method. A mixture of 500 μL of NGS-PEG (2 mg/mL), ∼800 μCi Na[125]I and 100 μL of 4 mg/mL chloramine-T (Sigma-Aldrich) was reacted in a pH 7.5 phosphate buffer (0.02 M) for 30 min at room temperature. Excess ^{125}I was completely removed by centrifugation filtration through Amicon filters (MWCO = 100 kDa) and washed away with water for 4−6 times until no detachable gamma activity in the filtrate solution. A radiolabeling yield of 50−60% was achieved. In a control experiment, Na[125]I was mixed with NGS-PEG without addition of chloramine T. Nearly zero radioactivity was left after washing, suggesting that ^{125}I was covalently conjugated to graphene instead of physical adsorption. ^{125}I-NGS-PEG was injected into mice in the 0.9% NaCl saline solution.

Radiolabeling Stability Test. An approximate 5 μL portion of ^{125}I-NGS-PEG (0.5 mg/mL) was mixed with 400 μL of 0.9% sodium chloride, fetal bovine serum, and mouse plasma at 37 °C in a water bath. Free iodine was removed by centrifuge filtration through Amicon centrifugal filters (MWCO = 10 kDa) and washed with water for two times. The leftover ^{125}I-NGS-PEG after washing was collected for gamma counting to measure the amount of retained ^{125}I on graphene. Control experiments showed that over 99% of detached free ^{125}I could be effectively removed by this method.

Blood Circulation and Biodistribution of ^{125}I-Labeled NGS-PEG. Healthy female Balb/c mice were purchased from Suzhou Industrial Park Animal Technology Co., Ltd. All animal experiments were conducted under protocols approved by the Soochow University Laboratory Animal Center. Blood circulation was measured by drawing *ca.* 10 μL blood from the tails of Balb/c mice postinjection of ^{125}I-NGS-PEG. The concentration of ^{125}I-NGS-PEG in the blood was determined by using a gamma counter (Science and Technology Institute of China in Jia Branch Innovation Co., Ltd.). A series of dilutions of the ^{125}I-NGS-PEG solutions were measured to obtain a standard calibration curve. For biodistribution measurement, mice injected with ^{125}I-NGS-PEG were sacrificed at various time points with major organs collected for gamma counting. All biodistribution data were decay corrected by the half-life of [125]I (60 days). Statistics were based on standard deviations of 4−5 mice per group.

Blood Analysis and Histology Examinations. Twenty-five Healthy female Balb/c mice were injected with 200 μL of 2 mg/mL NGS-PEG (a dose of 20 mg/kg) and sacrificed at various time points after injection (3, 7, 20, 40, and 90 days, five mice per time point). Other 15 healthy Balb/c mice were used as the untreated control and sacrificed at 3, 40, and 90 days p.i. (five mice per time points). An approximate 0.8 mL portion of blood from each mouse was collected for a blood chemistry test and complete blood panel analysis before the mouse was euthanized. The serum chemistry data and complete blood panel were measured in the Shanghai Research Center for Biomodel Organism. Major organs from those mice were harvested, fixed in 4% neutral buffered formalin, processed routinely into paraffin, sectioned at 8 μm, stained with hematoxylin and eosin (H&E) and examined by a digital microscope (Leica QWin). Examined tissues include liver, kidneys, spleen, heart, lung, and intestine. Statistics were based on standard deviations of 5 mice per group.

Supporting Information Available: Additional figures and data as described in the text. This material is available free of charge *via* the Internet at http://pubs.acs.org.

REFERENCES AND NOTES

1. Cai, W. B.; Chen, X. Y. Nanoplatforms for Targeted Molecular Imaging in Living Subjects. *Small* **2007**, *3*, 1840–1854.
2. Ferrari, M. Cancer Nanotechnology: Opportunities and Challenges. *Nat. Rev. Cancer* **2005**, *5*, 161–171.
3. Farokhzad, O. C.; Langer, R. Nanomedicine: Developing Smarter Therapeutic and Diagnostic Modalities. *Adv. Drug Delivery Rev.* **2006**, *58*, 1456–1459.
4. Lacerda, L.; Bianco, A.; Prato, M.; Kostarelos, K. Carbon Nanotubes as Nanomedicines: From Toxicology to Pharmacology. *Adv. Drug Delivery Rev.* **2006**, *58*, 1460–1470.
5. Hauck, T. S.; Anderson, R. E.; Fischer, H. C.; Newbigging, S.; Chan, W. C. W. *In Vivo* Quantum-Dot Toxicity Assessment. *Small* **2010**, *6*, 138–144.
6. Schipper, M. L.; Nakayama-Ratchford, N.; Davis, C. R.; Kam, N. W. S.; Chu, P.; Liu, Z.; Sun, X.; Dai, H.; Gambhir, S. S. A Pilot Toxicology Study of Single-Walled Carbon Nanotubes in a Small Sample of Mice. *Nat. Nanotechnol.* **2008**, *3*, 216–221.
7. Li, X. L.; Wang, X. R.; Zhang, L.; Lee, S. W.; Dai, H. J. Chemically Derived, Ultrasmooth Graphene Nanoribbon Semiconductors. *Science* **2008**, *319*, 1229–1232.
8. Geim, A. K.; Novoselov, K. S. The Rise of Graphene. *Nat. Mater.* **2007**, *6*, 183–191.
9. Geim, A. K. Graphene: Status and Prospects. *Science* **2009**, *324*, 1530.
10. Wu, H. C.; Chang, X. L.; Liu, L.; Zhao, F.; Zhao, Y. L. Chemistry of Carbon Nanotubes in Biomedical Applications. *J. Mater. Chem.* **2010**, *20*, 1036–1052.

11. Kostarelos, K.; Bianco, A.; Prato, M. Promises, Facts and Challenges for Carbon Nanotubes in Imaging and Therapeutics. *Nat. Nanotechnol.* **2009**, *4*, 627–633.

12. Liu, Z.; Tabakman, S. M.; Chen, Z.; Dai, H. Preparation of Carbon Nanotube Bioconjugates for Biomedical Applications. *Nat. Protoc.* **2009**, *4*, 1372–1382.

13. Liu, Z.; Fan, A.; Rakhra, K.; Sherlock, S.; Goodwin, A.; Chen, X.; Yang, Q.; Felsher, D.; Dai, H. Supramolecular Stacking of Doxorubicin on Carbon Nanotubes for *In Vivo* Cancer Therapy. *Angew. Chem., Int. Ed.* **2009**, *48*, 7668–7672.

14. Liu, Z.; Tabakman, S.; Welsher, K.; Dai, H. Carbon Nanotubes in Biology and Medicine: *In Vitro* and *in Vivo* Detection, Imaging and Drug Delivery. *Nano Res.* **2009**, *2*, 85–120.

15. Xu, X. A.; Jiang, S. J.; Hu, Z.; Liu, S. Q. Nitrogen-Doped Carbon Nanotubes: High Electrocatalytic Activity toward the Oxidation of Hydrogen Peroxide and Its Application for Biosensing. *ACS Nano* **2010**, *4*, 4292–4298.

16. Zeng, Z. Y.; Zhou, X. Z.; Huang, X. A.; Wang, Z. J.; Yang, Y. L.; Zhang, Q. C.; Boey, F.; Zhang, H. Electrochemical Deposition of Pt Nanoparticles on Carbon Nanotube Patterns for Glucose Detection. *Analyst* **2010**, *135*, 1726–1730.

17. Huang, Y. X.; Palkar, P. V.; Li, L. J.; Zhang, H.; Chen, P. Integrating Carbon Nanotubes and Lipid Bilayer for Biosensing. *Biosens. Bioelectron.* **2010**, *25*, 1834–1837.

18. Liu, X.; Tao, H.; Yang, K.; Zhang, S.; Lee, S.-T.; Liu, Z. Optimization of Surface Chemistry on Single-Walled Carbon Nanotubes for *in Vivo* Photothermal Ablation of Tumors. *Biomaterials* **2011**, *32*, 144–151.

19. He, S.; Song, B.; Li, D.; Zhu, C.; Qi, W.; Wen, Y.; Wang, L.; Song, S.; Fang, H.; Fan, C. A Graphene Nanoprobe for Rapid, Sensitive, and Multicolor Fluorescent DNA Analysis. *Adv. Funct. Mater.* **2010**, *20*, 453–459.

20. Jung, J. H.; Cheon, D. S.; Liu, F.; Lee, K. B.; Seo, T. S. A Graphene Oxide Based Immuno-Biosensor for Pathogen Detection. *Angew. Chem., Int. Ed.* **2010**, 1–5.

21. Choi, B. G.; Park, H.; Park, T. J.; Yang, M. H.; Kim, J. S.; Jang, S. Y.; Heo, N. S.; Lee, S. Y.; Kong, J.; Hong, W. H. Solution Chemistry of Self-Assembled Graphene Nanohybrids for High-Performance Flexible Biosensors. *ACS Nano* **2010**, *4*, 2910–2918.

22. Lu, C.-H.; Zhu, C.-L.; Li, J.; Liu, J.-J.; Chen, X.; Yang, H.-H. Using Graphene to Protect DNA from Cleavage during Cellular Delivery. *Chem. Commun.* **2010**, *46*, 3116–3118.

23. Tang, L. A. L.; Wang, J.; Loh, K. P. Graphene-Based SELDI Probe with Ultrahigh Extraction and Sensitivity for DNA Oligomer. *J. Am. Chem. Soc.* **2010**, *132*, 10976–10977.

24. He, Q. Y.; Sudibya, H. G.; Yin, Z. Y.; Wu, S. X.; Li, H.; Boey, F.; Huang, W.; Chen, P.; Zhang, H. Centimeter-Long and Large-Scale Micropatterns of Reduced Graphene Oxide Films: Fabrication and Sensing Applications. *ACS Nano* **2010**, *4*, 3201–3208.

25. Wang, Z. J.; Zhou, X. Z.; Zhang, J.; Boey, F.; Zhang, H. Direct Electrochemical Reduction of Single-Layer Graphene Oxide and Subsequent Functionalization with Glucose Oxidase. *J. Phys. Chem. C* **2009**, *113*, 14071–14075.

26. Wang, Y.; Shao, Y. Y.; Matson, D. W.; Li, J. H.; Lin, Y. H. Nitrogen-Doped Graphene and Its Application in Electrochemical Biosensing. *ACS Nano* **2010**, *4*, 1790–1798.

27. Sun, X.; Liu, Z.; Welsher, K.; Robinson, J. T.; Goodwin, A.; Zaric, S.; Dai, H. Nanographene Oxide for Cellular Imaging and Drug Delivery. *Nano Res.* **2008**, *1*, 203–212.

28. Liu, Z.; Robinson, J. T.; Sun, X. M.; Dai, H. J. PEGylated Nanographene Oxide for Delivery of Water-Insoluble Cancer Drugs. *J. Am. Chem. Soc.* **2008**, *130*, 10876–10877.

29. Zhang, L.; Xia, J.; Zhao, Q.; Liu, L.; Zhang, Z. Functional Graphene Oxide as a Nanocarrier for Controlled Loading and Targeted Delivery of Mixed Anticancer Drugs. *Small* **2009**, *6*, 537–544.

30. Yang, X.; Zhang, X.; Liu, Z.; Ma, Y.; Huang, Y.; Chen, Y. High-Efficiency Loading and Controlled Release of Doxorubicin Hydrochloride on Graphene Oxide. *J. Phys. Chem. C* **2008**, 17554–17558.

31. Yang, K.; Zhang, S.; Zhang, G.; Sun, X.; Lee, S. T.; Liu, Z. Graphene in Mice: Ultrahigh *In Vivo* Tumor Uptake and Efficient Photothermal Therapy. *Nano Lett.* **2010**, *10*, 3318–3323.

32. Wang, H.; Wang, J.; Deng, X.; Sun, H.; Shi, Z.; Gu, Z.; Liu, Y.; Zhao, Y. Biodistribution of Carbon Single-Wall Carbon Nanotubes in Mice. *J. Nanosci. Nanotechnol.* **2004**, *4*, 1019–1024.

33. Liu, Z.; Davis, C.; Cai, W.; He, L.; Chen, X.; Dai, H. Circulation and Long-Term Fate of Functionalized, Biocompatible Single-Walled Carbon Nanotubes in Mice Probed by Raman Spectroscopy. *Proc. Natl. Acad. Sci. U.S.A.* **2008**, *105*, 1410–1415.

34. Liu, Z.; Chen, K.; Davis, C.; Sherlock, S.; Cao, Q.; Chen, X.; Dai, H. Drug Delivery with Carbon Nanotubes for *in Vivo* Cancer Treatment. *Cancer Res.* **2008**, *68*, 6652–6660.

35. Reference ranges of hematology data of healthy female Balb/c mice were obtained from Charles River Laboratories: http://www.criver.com/EN-US/PRODSERV/BYTYPE/RESMODOVER/RESMOD/Pages/BALBcMouse.aspx.